THE BUCKLING OF A THIN PLATE DUE TO THE PRESENCE OF AN EDGE DISLOCATION

von

R. Siems, P. Delavignette u. S. Amelinckx

Solid State Physics Department, S.C.K.—C.E.N., Mol

The Buckling of a Thin Plate due to the Presence of an Edge Dislocation

By

R. Siems [1]), P. Delavignette and S. Amelinckx

It is shown that an edge dislocation parallel to the surface of a thin foil causes buckling of this foil by an angle of about $\theta = b/t$. (b = Burgers vector; t = thickness of the foil). The angle θ depends on the position of the dislocation. It is maximum for a dislocation in the middle of the foil and it tends to zero as the dislocation approaches to the surface. It is shown that the buckling is responsible for the discontinuous change in contrast along a dislocation as observed in transmission electron microscopy. The sense of buckling which can be determined by means of Kikuchi lines depends on the sign of the dislocation. The effect therefore provides an easy means to determine the *sign* of edge dislocations.

Es wird gezeigt, daß eine parallel zur Oberfläche einer dünnen Schicht liegende Stufen-versetzung zu einer Verbiegung der Schicht um einen Winkel $\theta = b/t$ Veranlassung gibt (b = Burgersvektor, t = Dicke der Schicht). Der Winkel θ ist maximal für eine Versetzung in der Mitte der Schicht und strebt gegen Null, wenn sich die Versetzung der Oberfläche nähert. Es wird gezeigt, daß die Verbiegung für die unstetige Kontraständerung verant-wortlich ist, die bei elektronenmikroskopischer Untersuchung entlang einer Versetzung auftritt. Die Richtung der Verschiebung, die sich mit Hilfe von Kikuchi-Linien bestimmen läßt, hängt vom Vorzeichen der Versetzung ab. Dieser Effekt kann ausgenutzt werden, um in einfacher Weise das Vorzeichen von Stufenversetzungen zu bestimmen.

1. Introduction

Eshelby [1] has shown that a screw dislocation along the axis of a thin rod causes a lattice twist which may become notable in very thin rods, for instance in whiskers [2, 3]. The effect is due to the existence of image forces as a consequence of the finite size of the body.

Also, it is easy to see intuitively that an edge dislocation in a thin platelet, parallel to its surface, causes buckling. It is the purpose of this paper to estimate the magnitude of the effect and to present evidence that it leads to effects observable in the electron microscope; in particular, the phenomenon explains some contrast effects described previously [4].

Furthermore, it will be shown how detailed information can be obtained by a combination of electron microscopy and diffraction.

2. Estimate of the Angle of Buckling

It is easy to make an order of magnitude estimate for the angle θ by considering the case of a pure symmetrical tilt boundary. The angle of misorientation θ is given by b/D where b is the Burgers vector of the edge dislocation, and D the distance between dislocations. Taking $D = t$, the thickness of the plate will yield an order of magnitude estimate which is not too bad if the dislocation is in the middle of the plate.

---

[1]) Permanent address: K.F.A., Jülich, Institut für Reaktorwerkstoffe

This estimate appears justified by the observation that all along the planes, perpendicular to the tilt boundary and bisecting the distance between two dislo-cations, the stresses τ_{xx} and τ_{yy} vanish. The stress τ_{yx} also disappears along these planes at a sufficiently large distance from the boundary plane [5]. Let us consi-der now a bicrystal containing a pure tilt boundary according to the model of Fig. 1. There are no far reaching stresses in such a body. Let us now cut out a platelet limited by the planes $x = \pm D/2$. We have just seen that along these planes all stresses vanish; such platelets will therefore have stress-free surfaces, except for τ_{yx} in the immediate vicinity of the dislocation. The platelet will be buckled over an angle $\theta = b/D$.

A detailed calculation is required if the dislocation is not in the middle of the platelet; this is done in the next paragraph.
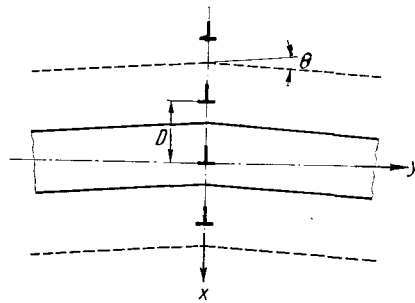

Fig. 1. Diagram illustrating the relation between a symmetrical tilt boundary in an infinite solid and a platelet containing a single edge dislocation (full line) parallel to the surface

3. Calculation of the Angle of Buckling

Let an edge dislocation be situated a distance ξ under the surface of a plate of isotropic material. We ask for the angle $\theta = 2\,\Theta$ (Fig. 2) through which the plate is bent due to the presence of the dislocation. This angle is given in terms of the difference Δv in displacement (in the y-direction) between the upper and lower surfaces:

$$\Theta \approx \sin \Theta = \frac{\Delta v}{t}\,. \tag{1}$$

According to Hooke's law for the case of plane stress

$$\frac{\partial v}{\partial y} = \frac{1}{2\,\mu}\{\tau_{yy}\,(1-\nu) - \nu\,\tau_{xx}\}\,. \tag{2}$$

The problem of the stress field around a dislocation in a plate was treated by Dietze and Leibfried [6]. They started with the stress field of a dislocation in infinite material and compensated the surface value of the τ_{xy} component of this stress field by an infinite series of mirror dislocations (see Fig. 3).

The stress field due to these dislocations can be given in a closed form. The components τ_{xx} remaining at the two surfaces are

$$
\left.
\begin{aligned}
x = 0: \quad \tau_{xx}^0 &= K\left\{\frac{1}{\cosh Y - \cos \Xi} - \frac{Y \sinh Y}{(\cosh Y - \cos \Xi)^2}\right\}, \\
x = t: \quad \tau_{xx}^t &= -K\left\{\frac{1}{\cosh Y + \cos \Xi} - \frac{Y \sinh Y}{(\cosh Y + \cos \Xi)^2}\right\},
\end{aligned}
\right\} \tag{3}
$$

with

$$X = \pi\frac{x}{t}\,, \qquad Y = \pi\frac{y}{t}\,, \qquad \Xi = \pi\frac{\xi}{t}\,, \qquad K = \frac{b}{2\pi}\frac{\mu}{1-\nu}\frac{\pi}{t}\sin \Xi\,.$$

Fig. 2. Buckling of thin plate due to the presence of an edge dislocation. The drawing illustrates the notations used. The dashed line is the unbent plate whilst the full line is the stress free bent plate
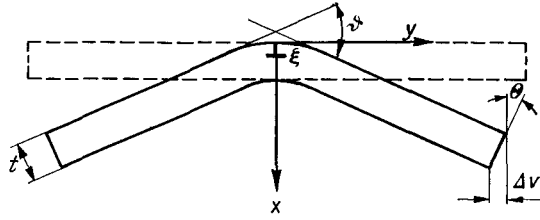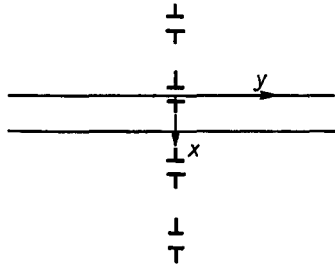
Fig. 3. Some of the mirror dislocations used to calculate the stress field due to an edge dislocation in a thin platelet

So far, because of the symmetry of the arrangement in Fig. 3, there is no bending. To make the surfaces tress-free, a stress field has to be superposed which compensates the surface stresses (3). This stress field is responsible for the bending. It is derived from a stress function F which has to obey the bipotential equation $\Delta\Delta F = 0$. This is ensured by expressing F in terms of two potential functions χ and ω.

$$F = x\,\chi_x - \chi + (t - x)\,\omega_x + \omega \,. \tag{4}$$

As χ and ω are potential functions, they may be written in the form

$$\chi = \int_{-\infty}^{\infty} c(m) \sinh m\,(\pi - X)\, e^{imY}\, dm \,, \qquad \omega = \int_{-\infty}^{\infty} d(m) \sinh m\, X\, e^{imY}\, dm \,.$$

$c(m)$ and $d(m)$ are so chosen that the surface stresses (3) are compensated. In this way DIETZE and LEIBFRIED obtain integral expressions for χ and ω:

$$
\left.
\begin{aligned}
\chi(X, Y) &= A\, t \int_{-\infty}^{\infty} \frac{\sinh m\,\pi\, \dfrac{\partial}{\partial m}\left\{\dfrac{\sinh m\,(\pi - \varXi)}{\sinh m\,\pi}\right\} + m\,\pi\, \dfrac{\partial}{\partial m}\left\{\dfrac{\sinh m\,\varXi}{\sinh m\,\pi}\right\}}{\sinh^2 m\,\pi - (m\,\pi)^2} \\
&\qquad \times \frac{\sinh m\,(\pi - X)}{m\,\pi} \cos m\, Y\, dm \,, \\[2mm]
\omega(X, Y) &= A\, t \int_{-\infty}^{\infty} \frac{\sinh m\,\pi\, \dfrac{\partial}{\partial m}\left\{\dfrac{\sinh m\,\varXi}{\sinh m\,\pi}\right\} + m\,\pi\, \dfrac{\partial}{\partial m}\left\{\dfrac{\sinh m\,(\pi - \varXi)}{\sinh m\,\pi}\right\}}{\sinh^2 m\,\pi - (m\,\pi)^2} \\
&\qquad \times \frac{\sinh m\, X}{m\,\pi} \cos m\, Y\, dm \,,
\end{aligned}
\right\} \tag{5}
$$

where A is given by $A = \dfrac{b}{2\,\pi} \dfrac{\mu}{1 - \nu}$.

These expressions could not be integrated to obtain the stresses[2]. We could, however, obtain an expression for the asymptotic $(y \to \infty)$ value of the angle Θ.

According to equation (2)

$$\Delta v(Y) = v^0(Y) - v^i(Y) = \frac{1}{2\,\mu}\,\frac{t}{\pi}\int_0^Y \{(1-\nu)\,\Delta\tau_{yy} - \nu\,\Delta\tau_{xx}\}\,dY\,. \tag{6}$$

Introducing for $-\tau_{xx}$ the values from (3) we obtain

$$\frac{t}{\pi}\int_0^Y \Delta\tau_{xx}\,dY = -K\,\frac{t}{\pi}\left[\frac{Y}{\cosh Y - \cos \Xi} + \frac{Y}{\cosh Y + \cos \Xi}\right]\,;\quad \lim_{Y \to \infty}\int_0^Y \Delta\tau_{xx}\,dY = 0\,.$$

The only contribution to the bending is therefore contained in the first term of (6). According to (4)

$$\tau_{yy} = F_{xx} = x\,\chi_{xxx} + \chi_{xx} + (t-x)\,\omega_{xxx} - \omega_{xx}\,,$$

i.e.

$$\frac{t}{\pi}\int_0^Y \Delta\tau_{yy}\,dY = A\int_{-\infty}^\infty \frac{m^2\,\pi^2}{t\,(\sinh m\,\pi - m\,\pi)}\,\frac{\partial}{\partial m}\left\{\frac{\sinh m\,(\pi - \Xi) + \sinh m\,\Xi}{\sinh m\,\pi}\right\}$$
$$\times\left\{\frac{\sinh m\,\pi}{m\,\pi} + 1\right\}t\,\frac{\sin m\,Y}{m\,\pi}\,dm\,.$$

This integral has to be evaluated for large values of Y. Now

$$\lim_{Y \to \infty}\int_a^b \frac{\sin m\,Y}{\pi\,m}f(m)\,dm = \begin{cases} f(0) & \text{for}\quad a\,b < 0 \\ 0 & \text{for}\quad a\,b > 0\,. \end{cases}$$

For $m \to 0$ the factor of $\dfrac{\sin m\,Y}{m\,\pi}$ in the above integrand approaches the value

$$12\,A\,\pi\cdot\frac{\Xi}{\pi}\left(\frac{\Xi}{\pi} - 1\right) = 12\,A\,\pi\cdot\frac{\xi}{t}\left(\frac{\xi}{t} - 1\right)\,.$$

From equation (6) we obtain

$$\Delta v = \frac{3}{4}\,b\cdot 4\,\frac{\xi}{t}\left(\frac{\xi}{t} - 1\right)\,.$$

The bending angle $\Theta = 2\,\Theta$ is then

$$\Theta = \frac{6\,b\,\xi}{t^3}\,(\xi - t)\,. \tag{7}$$

The average relative depth from the nearest surface is $\dfrac{\xi}{t} = \dfrac{1}{4}$. For a dislocation in this position we obtain

$$|\Theta| = \frac{9}{8}\,\frac{|b|}{t}\,. \tag{8}$$

---

[2]) The integrals for χ and ω do not converge because of the singularity of the integrands at $m = 0$. This is, however, not a serious handicap, as the expressions for F_x and F_y obtained by formal differentiation under the integral sign are finite and the stresses obtained therefrom have the correct values at the surfaces.

Remark

At first glance it may, perhaps, seem strange that the bend angle for a dislocation in the middle of a plate is larger than the bend angle b/t for a low angle boundary with dislocation spacing $D = t$.

One may, however, see that this result is reasonable. Bending by an angle b/t can be produced by cutting the plate normal to the surface and inserting a wedge of height t and thickness b (Fig. 4a).
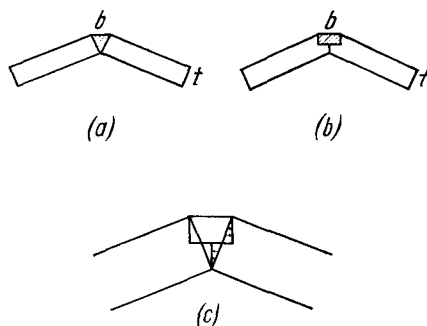

Fig. 4. Intuitive picture to show why the bending angle is somewhat larger for a thin plate containing an edge dislocation than for the corresponding tilt boundary.

a) A triangular wedge of which the base has length b is inserted in the gap and produces the bending angle $\alpha \approx b/t$ as in the tilt boundary

b) A small block of thickness b and heigth $t/2$ is inserted. This is the situation valid for a plate with a dislocation in the middle

c) Displacement of the interface on deforming the wedge shaped insert of (a) into the block shaped insert of (b). Notice that the bent angle increases

The bending due to a dislocation in the middle of the plate, on the other hand, is produced by cutting the plate only half way through and inserting a sheet of material of height $t/2$ and thickness b (Fig. 4b). In Fig. 4c the movement of the right boundary upon deformation of the inserted piece from wedge to sheet is indicated. One observes that the average motion in the upper half is to the right, in the lower part to the left. This corresponds to an increase in bend angle.

4. Contrast due to the Buckling

4.1 Non-absorbing crystals

We will now show that the sudden change in shade observed in many electron micrographs of layer crystals as shown in Fig. 5 is due to the buckling effect described in the previous section. First, the change in s required to give optimum contrast will be estimated, and in the second place it will be shown that the angular difference between crystal blocks on both sides of the dislocation is sufficient to cause the required change is s.

Apart from a constant factor, the intensity I diffracted by a perfect crystal foil of thickness t is given, in the dynamical two-beam approximation, by the following expression

$$I_s \cong \left[\sin^2 \pi \frac{t}{t_0} \sqrt{1 + (s\,t_0)^2} \right] \bigg/ [1 + (s\,t_0)^2] \tag{9}$$

where s is the "interference error"; it is a small vector measuring the distance of the center of gravity of the reciprocal lattice point to the Ewald sphere; t_0 is the extinction depth. A graph of I_s versus s, for a typical value of $t/t_0 = 3$, is shown in Fig. 6a.

The zero's of this function, which are at the same time the minima, are given by

$$s_{1,k} = \pm [k^2/t^2 - 1/t_0^2]^{1/2}, \tag{10}$$
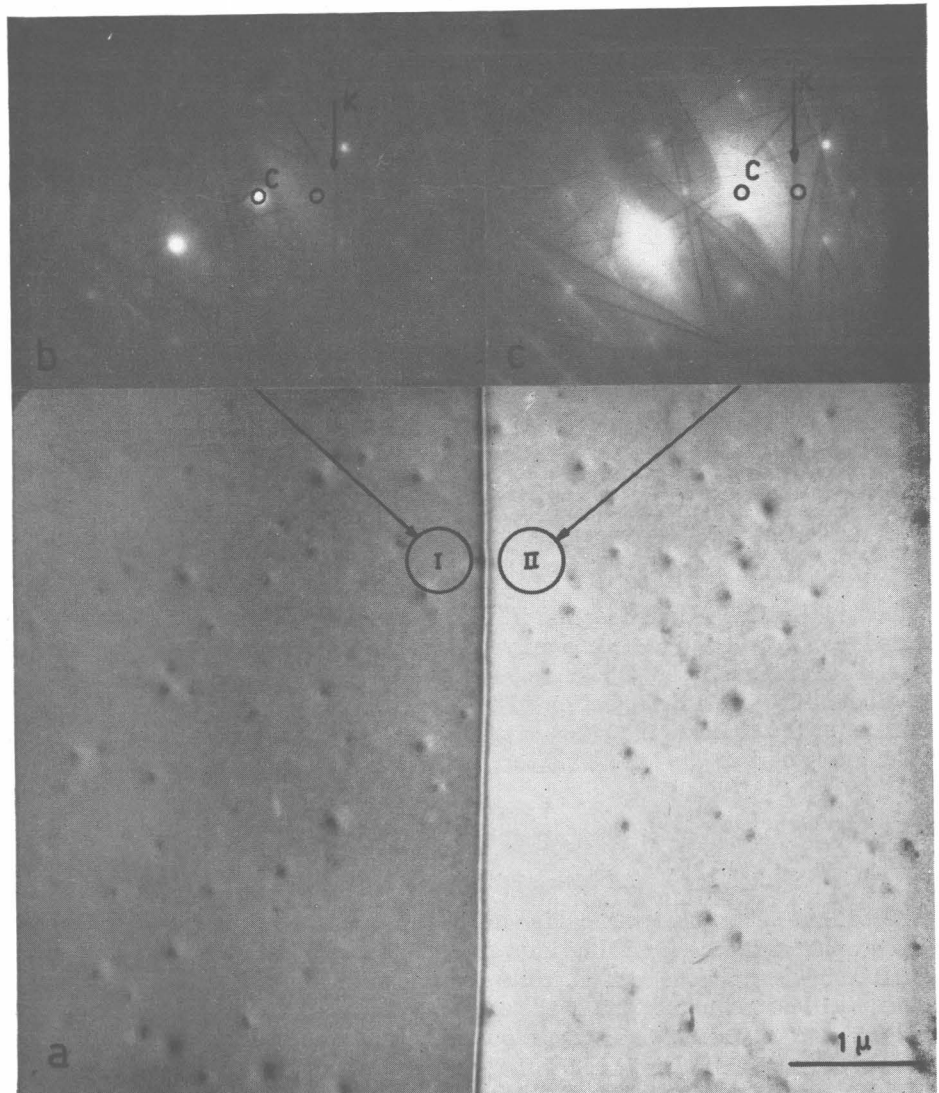
where k is an integer.

28*

Fig. 5. a) Striking discontinuous changes in transmitted intensity both sides of a dislocation in tin disulfide. (The contrast of the negative has been considerably suppressed on reproduction)

b) and c) Diffraction pattern taken left and right of the dislocation. The pattern in (b) was taken to reveal the Kossel-Möllenstedt fringes and allows to determine the foil thickness. The shift of the Kikuchi lines is also shown, it is exceptionally large here because the foil was thin; this was the reason why the photograph was selected
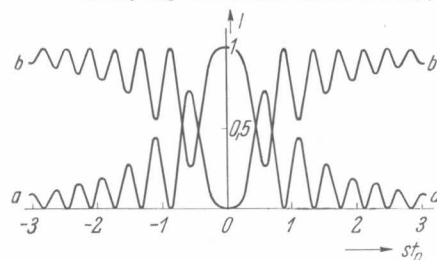

Fig. 6. Diffracted and transmitted intensity as a function of $s\,t_0$ for a crystal plate of thickness $t = 3\,t_0$, taking into account neither anomalous absorption nor normal absorption

a) diffracted intensity,
b) transmitted intensity

· The maxima are determined as solutions of the equation $x = \mathrm{tg}\, x$; for not too small values of s (or x), the solutions are approximately $x = (2\, k' + 1)\dfrac{\pi}{2}$ where k' is an integer, or

$$s_{2,k}{}' = \pm\, [(2\, k' + 1)^2/(4\, t^2 - 1/t_0^2)]^{1/2}\,. \tag{11}$$

The point $s = 0$ may correspond as well to a minimum as to a maximum, depending on the ratio t/t_0.

Since all minima, except perhaps the one at $s = 0$, are zero, and since furthermore the maxima decrease in magnitude, the optimum contrast between the two regions will be obtained if for one region the value of s corresponds to the first maximum, whereas in the other region the s-values correspond to a zero. The smallest possible $\varDelta s$ value giving rise to maximum contrast corresponds thus to the *next* zero.

Considering as a specific case $t = t_0$, one finds that the first maximum occurs for $s_1\, t_0 = \dfrac{1}{2}\,\sqrt{5}$ whereas the following minimum is for $s_2\, t_0 = \sqrt{3}$. For a change of $t_0\,\varDelta s = t_0\,(s_2 - s_1) = 0.62$ the contrast will be optimum. For other values of t, $t_0\,\varDelta s$ values of the same order of magnitude are found.

The relation between the change in orientation θ and $\varDelta s$ can be deduced immediately from

$$\varDelta s = \theta/d_{hkl}$$

or, taking for $\theta = b/t$ we obtain

$$t_0\,\varDelta s = t_0\,\theta/d_{hkl} = b\, t_0/t\, d_{hkl}\,. \tag{12}$$

For t_0/t of order 1 and $b/d_{hkl} \cong 1$, it is clear that $t_0\,\varDelta s$ should also be of order unity. It turns out that a change in s required for optimum contrast can easily occur in a foil of thickness t_0. With increasing thickness, smaller changes in $s\, t_0$ are sufficient to cause optimum contrast, since the minima of the curve of Fig. 6a become more closely spaced. However, a thickness increase also results in a decrease of the angle of buckling. Since the spacing of the minima goes roughly as $1/t$ (for large K) and hence the $t_0\,\varDelta s$ required for optimum contrast as t. Since, on the other hand, the bending angle goes as $1/t$, the contrast will not depend strongly on the thickness, according to the approximation used here.

The effect of using high-order reflections results in a decrease in d_{hkl} and an increase in t_0, and $t_0\,\varDelta s$ therefore increases for the same θ. One can therefore conclude that high-order reflections will produce a more pronounced contrast.

Visible contrast can therefore, of course, be obtained for a large number of combinations of s-values; it is sufficient that for one side of the dislocation the s-value corresponds approximately to zero intensity, whilst at the other side it gives rise to a reasonable diffracted intensity, i.e. is not too far from a maximum.

4.2 Influence of absorption

In thicker crystals the anomalous absorption may be important [7]. In this case the transmitted intensity is given approximately by the following expression [8]:

$$I_t = \left[\cosh \frac{\pi t}{\tau_0\,\sqrt{1 + (s\, t_0)^2}} + \frac{s\, t_0}{\sqrt{1 + (s\, t_0)^2}} \cdot \sinh \frac{\pi t}{\tau_0\,\sqrt{1 + (s\, t_0)^2}}\right]^2$$

$$- \frac{\sin^2 \pi \dfrac{t}{t_0}\,\sqrt{1 + (s\, t_0)^2}}{1 + (s\, t_0)^2}\,, \tag{13}$$
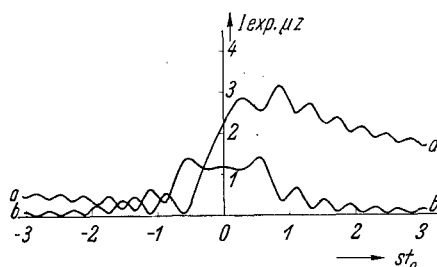
Fig. 7. Diffracted and transmitted intensity as a function of $s\,t_0$ for crystal plate of thickness $t = 3\,t_0$ taking into account anomalous absorption, but not normal absorption

a) diffracted intensity,
b) transmitted intensity

where $\tau_0 \cong 10\,t_0$ is the absorption length; higher powers of t_0/τ_0 have been neglected as well as the quantity

$$\frac{t_0}{\tau^0} \cdot \frac{1}{1 + (s\,t_0)^2} \cdot \frac{s\,t_0}{\sqrt{1 + (s\,t_0)^2}} \cdot \sin 2\pi \frac{t}{t_0}\sqrt{1 + (s\,t_0)^2} \,.$$

It is clear that expression (13) is asymmetrical in s, i.e. positive and negative s-values of the same magnitude produce quite different transmitted intensities. A typical curve, valid for a crystal of thickness $t = 3\,t_0$ is shown in Fig. 7a. A change in $s\,t_0$ of the order unity, in the neighbourhood of $s = 0$, produces maximum contrast.

The Fig. 7b shows the scattered intensity which is given by

$$I_s = \frac{\sinh^2 \dfrac{\pi t}{\tau_0 \sqrt{1 + (s\,t_0)^2}} + \sin^2 \dfrac{\pi t}{t_0}\sqrt{1 + (s\,t_0)^2}}{1 + (s\,t_0)^2} \,.$$

This curve is symmetrical in s. In order to demonstrate that absorption is important in causing the phenomenon, we observed the contrast for $s > 0$ and $s < 0$ in both bright and dark field ($11\bar{2}0$). In the bright field image, the same region (Fig. 8) is darker for both cases, whilst in the dark field image light and dark regions interchange. This is in accord with the curves of Fig. 7 but it would be difficult to explain this behaviour on the basis of the curves of Fig. 6, where no absorption was taken into account.

5. Quantitative Study of the Buckling

A detailed verification of formula (7) would require the knowledge of the foil thickness t, of the position of the dislocation ξ, as well as a determination of the angular difference θ and of the direction of the Burgers vector. It is also necessary to verify the sense of buckling as compared to the sign of the dislocation.

Unfortunately there is no convenient means to determine ξ. Should such a method become available, the formula (7) would provide a means of determining the magnitude of the Burgers vector.

5.1 Determination of the foil thickness

For metals one can make use of slip traces left by moving dislocations: such slip traces are localized at the upper and the lower face of the foil. If the orientation of the foil and the indices of the slip plane are known, the thickness t can be deduced from the width w of the slip trace. If φ is the angle between the normal to the foil and the normal to the slip plane, one has $t = w\,\mathrm{tg}\,\varphi$.

For layer structures this method cannot be applied, since the glide planes are strictly parallel to the foil plane. There is a purely electron-optical method which
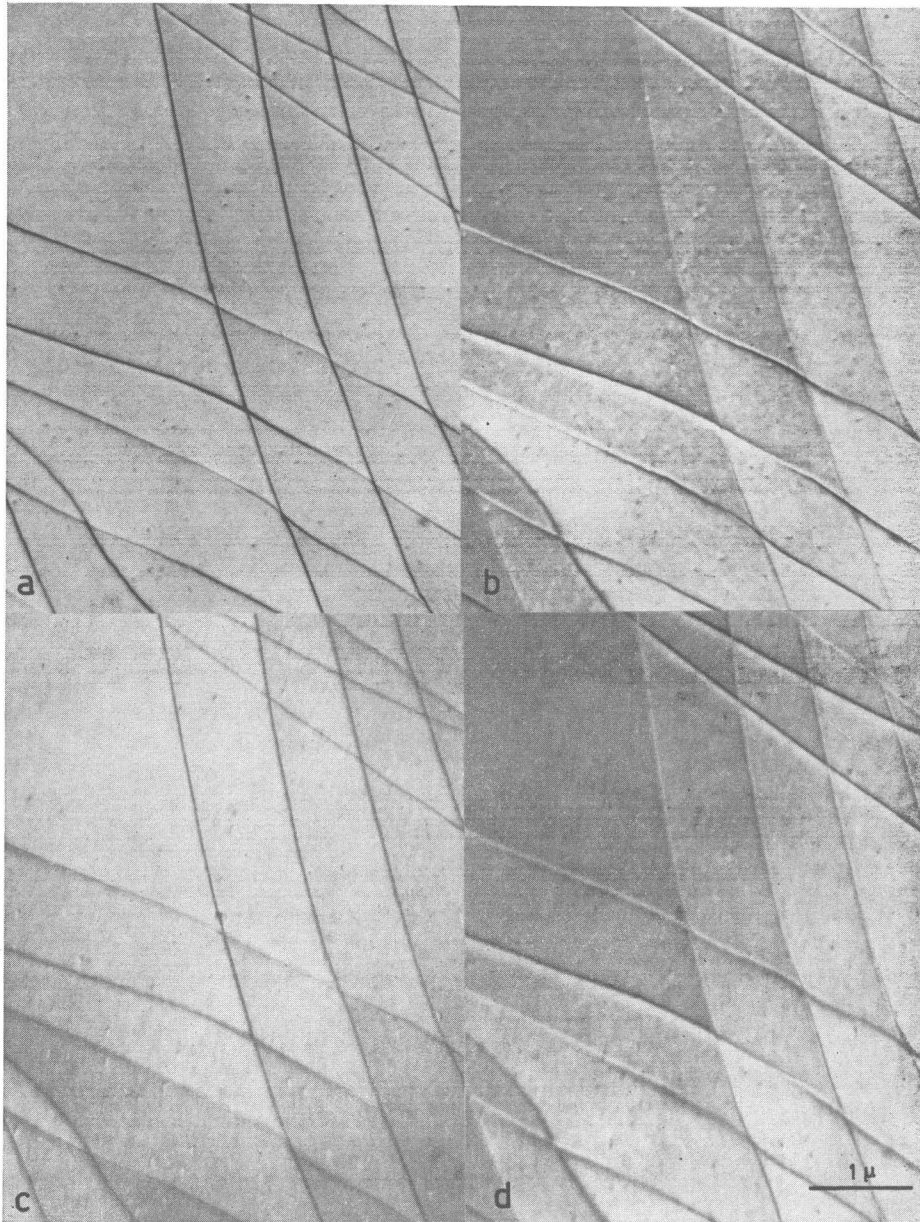
Fig. 8. Area containing several dislocations with edge character, taken under different contrast conditions:
$$s_1 > 0; \; s_2 < 0$$

a) bright field $s = s_1$
b) bright field $s = s_2$
c) dark field $s = s_1$
d) dark field $s = s_2$

Notice that the bright and dark sides are inverted for s-values of different sign in the dark field image, but not in the bright field image

is useful in such cases. The method makes use of the so-called Kossel and Möllen-
stedt fringes [9] which are due to the fine structure of the diffraction spots des-
cribed by (9). The fine structure is best revealed when admitting a slightly non-
parallel beam of electrons, by increasing the size of the condensor aperture. The
single Ewald sphere is now replaced by a set of Ewald spheres corresponding to
the different incident directions, and the whole intensity distribution along the
reciprocal lattice rod is explored. A striking example of such a pattern obtained
for graphite is shown in Fig. 9. The relation between Δs as measured along the
rod and Δx, the distance along the plate, is to a good approximation

$$\Delta s = \Delta x/(d_{hkl} + L),$$

where L is the effective distance specimen-plate, and d_{hkl} is the spacing of the
lattice planes. This relation allows to measure the Δs values directly on the plate.
It is sometimes a good approximation to use the kinematical theory, the equation
then reduces to

$$I(s, t) \cong \frac{\sin^2 \pi t s}{(\pi s)^2}. \tag{14}$$

The minima of this function are zero and they are equally spaced:

$$\Delta s = 1/t, \tag{15}$$

a determination of Δs for two successive fringes is thus equivalent to a thickness
measurement. This approximation is only valid far enough from the center of
gravity of the diffraction spot.

In the dynamical case, the minima are no longer equally spaced, and the deter-
mination of k (in (10)) becomes necessary. This can be done by determining the
s-values s_1, s_2, s_3 corresponding to three successive minima.

We can then write

$$\left.\begin{array}{l} 1 + (s_1 t_0)^2 = (k - 1)^2 (t_0/t)^2, \\ 1 + (s_2 t_0)^2 = k^2(t_0/t)^2, \\ 1 + (s_3 t_0)^2 = (k + 1)^2 (t_0/t)^2. \end{array}\right\} \tag{16}$$

When combining these three equations, one obtains

$$t = \sqrt{2}\,(s_1^2 + s_3^2 - 2\,s_2^2)^{-1/2}. \tag{17}$$

For a uniform spacing, this formula reduces evidently to relation (15) of the
kinematical case.

Further one finds $2\,k + 1 = (s_3^2 - s_2^2)\,t^2$ (18)

and a similar relation $2\,k - 1 = (s_2^2 - s_1^2)\,t^2,$ (19)

or even $4\,k = (s_3^2 - s_1^2)\,t^2.$ (20)

Knowing t from (17) and determining k from (18), (19) or (20) leads to a value
for t_0 from one of the relations (16). It should be noticed that k has to be an integer.
This enables to reduce the error on k, since one can choose the nearest integer
from a number of relations like (18), (19) and (20).

In practice one may try to find first a value for t by the use of relation (15) by
determining the spacing Δs sufficiently far from the center of gravity of the reci-
procal lattice point, where the kinematical theory should be applicable. This can
be judged experimentally if a uniform spacing is found. From t one can then pro-
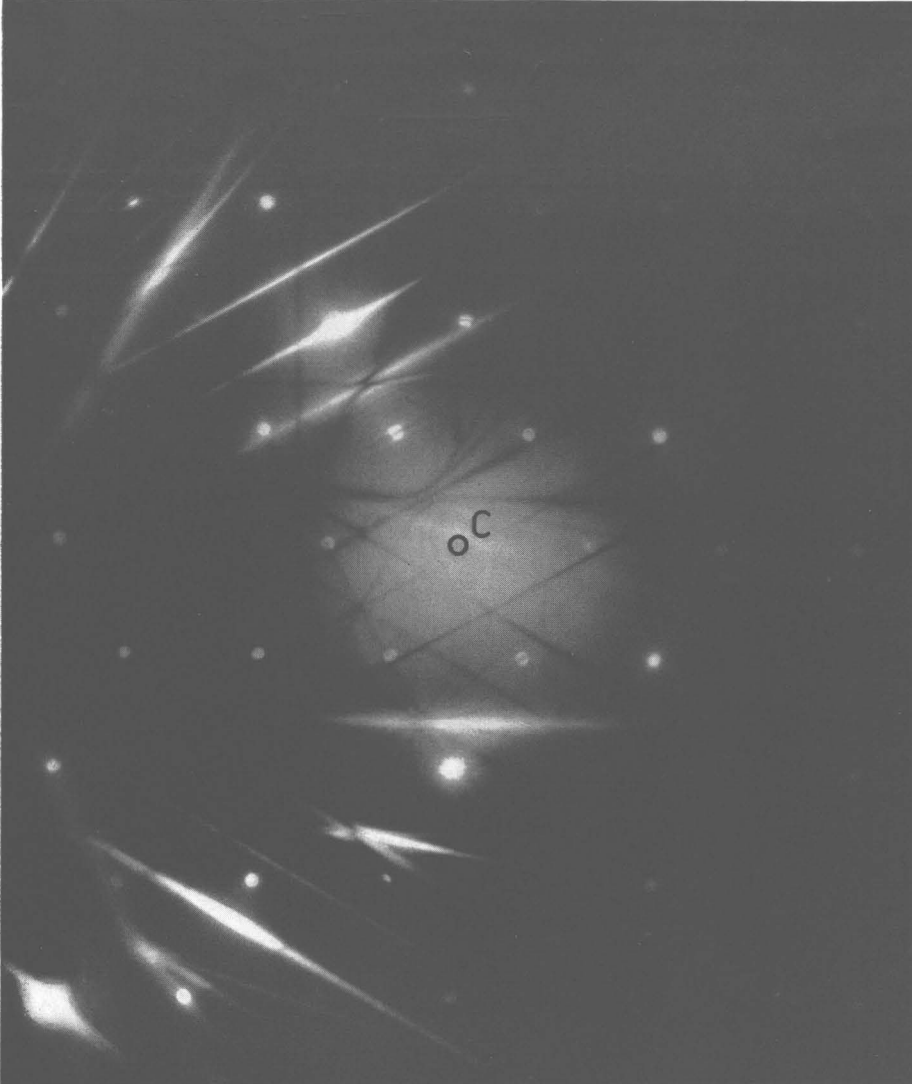ceed in the way outlined above.

Fig. 9. Kossel-Möllenstedt type fringes in a graphite flake to illustrate their use for thickness determinations. The spacing of the fringes in the different spots is inversely proportional to the distance from the center of the diagram of the considered spot. The crystal plate shown has a thickness of 1650 Å

5.2 The determination of Θ in magnitude and sign

For the measurement of θ use is made of selected area diffraction on both sides of the dislocation line. When moving the selected area across the dislocation line, a sudden shift Δc of the Kikuchi lines is noticed. The shift is largest for the Kikuchi lines parallel to the dislocation line. An example is seen in Fig. 10. Fig. 10c shows the pattern at one side of the dislocation, and Fig. 10d shows a similar pattern at the other side. The angle θ can be deduced directly from the shift

of the lines indicated with K: it is given by $\theta = \dfrac{\Delta c}{L}$. The measurement of L is usually avoided by the use of the following formula

$$\theta = \frac{\Delta c \cdot \lambda}{G \cdot d_{hkl}} , \tag{21}$$

where G is the distance of the diffraction spot $h\,k\,l$ to the center as measured on the plate. For the example shown, θ turns out to be 1.2×10^{-3} rad. The sense
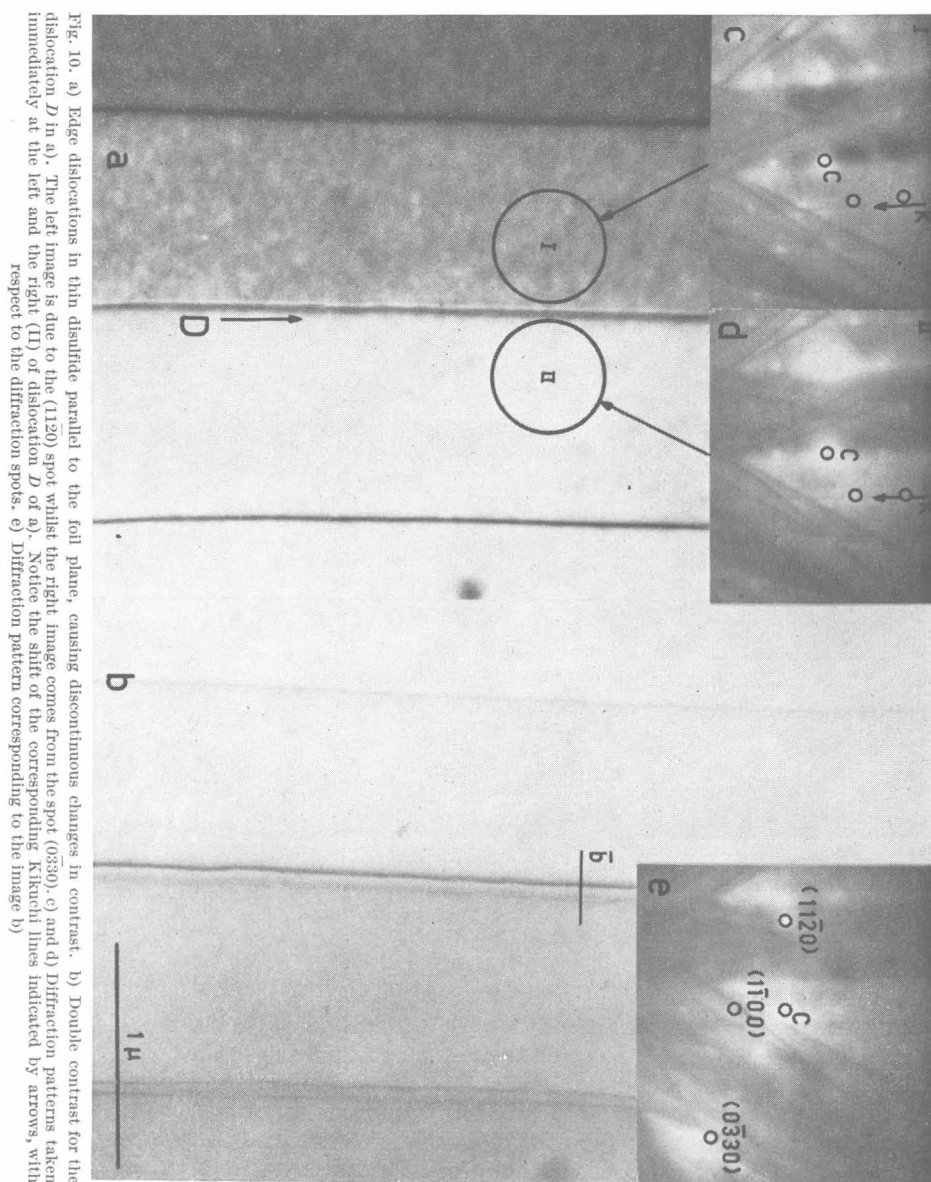

Fig. 10. a) Edge dislocations in thin disulfide parallel to the foil plane, causing discontinuous changes in contrast. b) Double contrast for the dislocation D in a). The left image is due to the (1120) spot whilst the right image comes from the spot (0330). c) and d) Diffraction patterns taken immediately at the left and the right (II) of dislocation D of a). Notice the shift of the corresponding Kikuchi lines indicated by arrows, with respect to the diffraction spots. e) Diffraction pattern corresponding to the image b)

of buckling follows directly from the sense of movement of the Kikuchi lines in going from one side of the dislocation to the other. This is shown schematically in Fig. 14.

5.3 Determination of the Burgers vector in direction and sense

The procedure used in determining the direction of the Burgers vector is based on the absence of contrast for $g \cdot \bar{b} = 0$ [10]. A practical method has been described previously for layer structures [11]. The dislocation shown in Fig. 10, which refers to SnS_2, is found to be pure edge. The dislocation goes out of contrast for a $(1\bar{1}00)$ type reflection, it is therefore concluded that it is perfect. The length of the shortest lattice vector having its direction in that plane is 3.64 Å; this is, therefore, the probable value of $|b|$.

In order to show that the buckling is in the sense required by the model, one must prove that the supplementary half plane of the edge dislocation is at the convex side of the foil. Making use of the one-sided nature of dislocation contrast, this can be done by comparing the sign of s with the image side of the dislocation. KELLY has applied such a procedure to the determination of the character of dislocation loops [12].

5.3.1 Determination of the sign of s

It is clear that if $s = 0$ for a given reflection $(h\ k\ l)$ the Kikuchi line due to the same reflection will pass exactly through the center of the corresponding spot $(h\ k\ l)$, which will strongly light up (Fig. 11 a).

Fig. 11. Relation between the position of a diffraction spot and the position of the Kikuchi line due to the same reflection:

a) $s = 0$. The reciprocal lattice point is on Ewald's sphere, if the Kikuchi line passes through the spot

b) $s > 0$. The reciprocal lattice point is inside Ewald's sphere if the Kikuchi line is further from the center than the spot

c) $s < 0$. The reciprocal lattice point is outside the reflecting sphere if the Kikuchi line is closer to the center than the spot

(a)   *(b)*   *(c)*
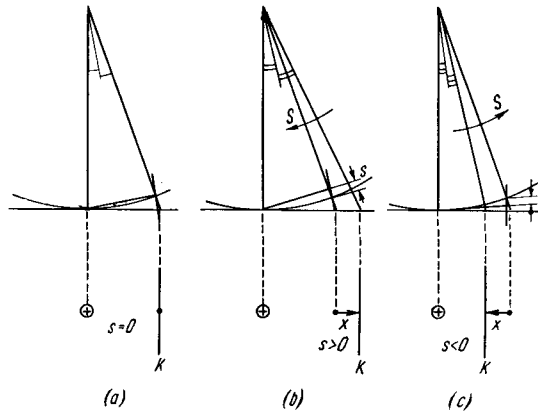
A rotation of the lattice in such a sense that the reciprocal lattice point moves out of Ewald's sphere will bring the Kikuchi lines nearer to the center of the diffraction pattern, and vice versa. Fig. 11 shows schematically the relative position of diffraction spot and Kikuchi lines for different situations: s has been called positive if the reciprocal lattice point is inside the sphere. The figure shows also the rotation S which turns the crystal into the Bragg condition.

The magnitude of s follows directly from the distance x measured on the plate; one has to a good approximation

$$s = \frac{x \cdot \lambda}{d^2_{h k l} \cdot G} ,$$ (22)

where λ is the wavelength of the electrons and x is the distance $(h\,k\,l)$ spot-Kikuchi line.

### 5.3.2 Determination of the image side

In the layer lattices it is easy to obtain double images due to two reflections producing contrast on opposite sides of the dislocations. The real position of the dislocation is clearly in between. One can also pass an extinction contour over the dislocation; the image then changes side. It is hence possible to determine the image side either by producing a double image or by comparing pictures with the image at different sides of the dislocation line, using surface features as reference marks.

5.3.3 The sign of $\overline{b}$

Combining the information from 5.3.1 and 5.3.2, one can determine the position of the supplementary halfplane by reference to Fig. 12 and 13.

The sign of s for the contrast-producing reflection tells us in which sense the lattice has to rotate in order to approach the Bragg condition. Suppose, for instance, that in the neighbourhood of the dislocation s is positive for a reflection to the right of the diffraction pattern; the sense of rotation of the lattice has then to be as shown by the arrow in Fig. 11 b. Fig. 12, on the other hand, shows the lattice rotation produced by edges and screws of both signs.

It is clear that the side of the dislocation where the senses of the two rotations coincide will be the image side. Applying this, for instance, to the positive edge dislocation shows that the image should be at the right. This type of reasoning allows to deduce the sign of the dislocation and hence the sense of the Burgers vector in all cases.


(a)   (b)

(c)   (d)
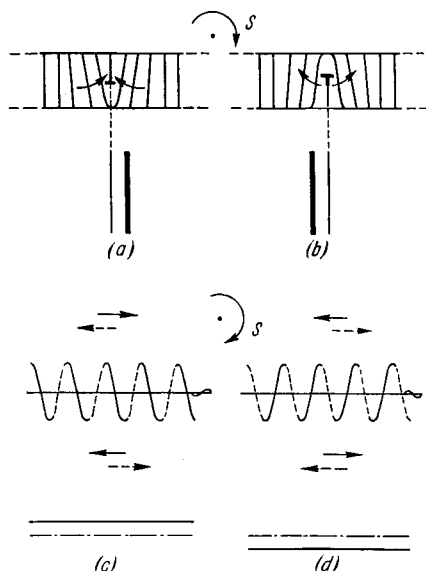
◀ Fig. 12. Relation between the sense of rotation of the lattice planes in the vicinity of the dislocation and the image side. The arrow S indicates the sense in which the lattice is rotated into the Bragg condition. S has to be deduced by the use of Fig. 11

    a) positive edge dislocation
    b) negative edge dislocation
    c) positive screw dislocation
    d) negative screw dislocation.

The dislocation configurations are drawn as projected on ABCD. The images are represented as projected on ABFE of Fig. 13

Fig. 13. Illustrating in space the meaning of Fig. 12. The edge dislocation e and the screw dislocation s are both shown in Fig. 12 projected on the plane ABCD ▼
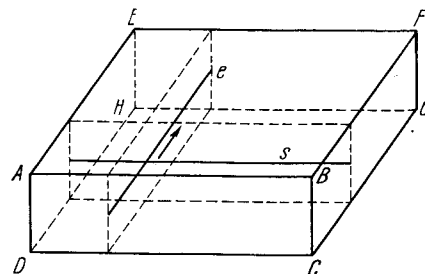
6. Observations

The considerations exposed above have been applied to dislocations in tindisul-fide and tinsulfoselenide platelets grown by sublimation. The crystals are usually rather perfect; isolated dislocations in undeformed regions, as required for the investigation, can easily be found. The crystals contain mostly ribbons, but also sometimes unextended dislocations. We reproduce here the observations neces-sary to make all the required measurements. A dislocation is chosen which is more or less parallel to the tilt axis of the specimen holder, since this simplifies the reasoning. We shall describe in detail one specific example for each measure-ment, but the experiment was made on several dislocations.

6.1 Direction of the Burgers vector

From the lack of contrast for a $(1\bar{1}00)$ reflection, the Burgers vector can be determined; it is as indicated (Fig. 10 b). Obviously the dislocation is almost pure edge.

6.2 Thickness of the foil

The fringes of Fig. 5 b allow to determine the foil thickness in the particular case shown: $t = 1.6 \times 10^{-5}$ cm.

6.3 Real position of the dislocation

Fig. 10 b shows for instance, a dislocation in double contrast with two different reflections operating: $(11\bar{2}0)$ and $(0\bar{3}30)$. By tilting it is easy to show that the image at the left is due to $(11\bar{2}0)$ and the image at the right to $(0\bar{3}30)$. Left and right are to be understood for an observer looking along the dislocation in the indicated sense. The corresponding diffraction pattern, oriented in the correct way with respect to the image, is shown as inset. The actual position of the dislo-cation is somewhere in between, in particular it is possible to conclude that the image due to the $(0\bar{3}30)$ reflection is at the right.

6.4 Relation image side-sign of s

From the diffraction pattern it is clear (Fig. 10 e) that the Kikuchi line is further from the center than the spot $(0\bar{3}30)$, i.e. we are in the case (b) of Fig. 11, and the sense of S is clockwise, as indicated. By consulting Fig. 12 it is found that the image will be at the right for a dislocation with supplementary half plane above the glide plane as in Fig. 12 a.

6.5 Sense and magnitude of orientation difference

Fig. 10 c and 10 d show the diffraction pattern immediately to the left and the right of the dislocation. The Kikuchi lines parallel to the dislocation, in particular, those indicated with arrows, shift discontinuously in passing the selection aperture over the dislocation. This can be judged from their position relative to the nearby spots. The Kikuchi line for the right part (II in Fig. 14 and 10) is clearly shifted to the left; i.e. we have the situation pictured in Fig. 14 a. The sense of buckling is concave downward in agreement with the sign of the Burgers vector. The orien-tation difference as computed from the shift corresponds within the limits set by the absence of a measured value for ξ to the theoretical value. Fig. 5 a illustrates a more striking example where the buckling was very pronounced as a consequence of the small value of $t = 1.6 \times 10^{-5}$ cm, as deduced from the Kossel-Möllenstedt
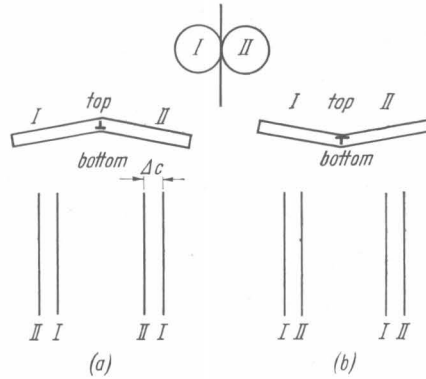
Fig. 14. Relation between the sense of buckling of the crystal plate and the relative position of the Kikuchi lines in region I and II, both sides of the dislocation. From their relative position the sense of buckling can be deduced

fringes (Fig. 5b). The orientation difference as computed from the shift of the Kikuchi lines is 4.5×10^{-3} rad, whilst the maximum theoretical value for $\xi = t/2$ is about 3.5×10^{-3} rad, which is evidently somewhat too small. This is probably due to some continuous bending, superposed on the discontinuous buckling.

Fig. 15 shows a particularly instructive observation: a dislocation line in a crystal of SnSSe. The dislocation is in the basal plane, but the surface is inclined at a very small angle with respect to the c-plane. The dislocation ends in the surface and goes gradually deeper at its other end. It is clear from Fig. 15a that as long as the dislocation is near to the surface there is no shade difference. Yet if the same contour is swept along the dislocation to the adjacent region, where the dislocation line goes deeper below the surface, the shade difference becomes rapidly more pronounced. This is evidently in agreement with the qualitative behaviour predicted by the formula (7).
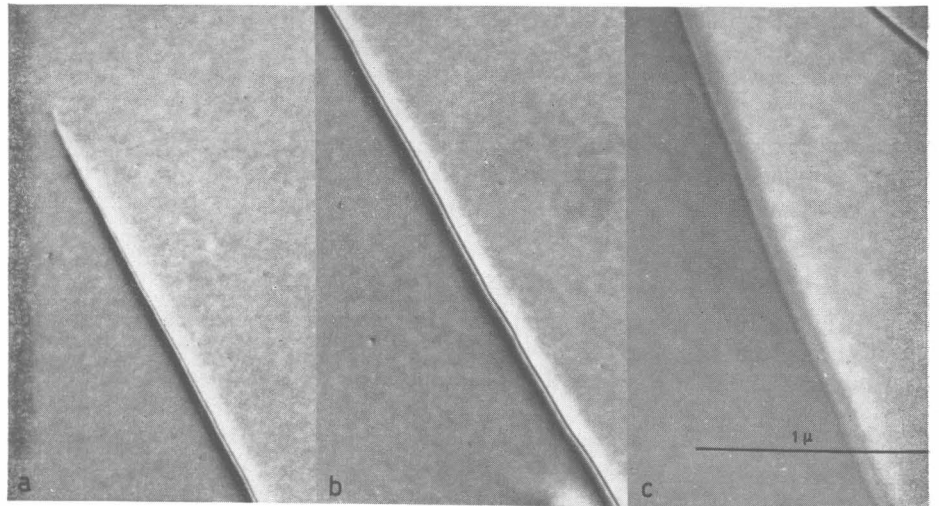

Fig. 15. Dislocation entering gradually deeper into the crystal, the dislocation is in the c-plane, but the upper surface of the crystal is slightly inclined with respect to the c-plane.

a) Emergence point in the surface
b) A small distance in the crystal; the contrast starts to become visible
c) At a sufficient distance in the crystal to produce a marked contrast
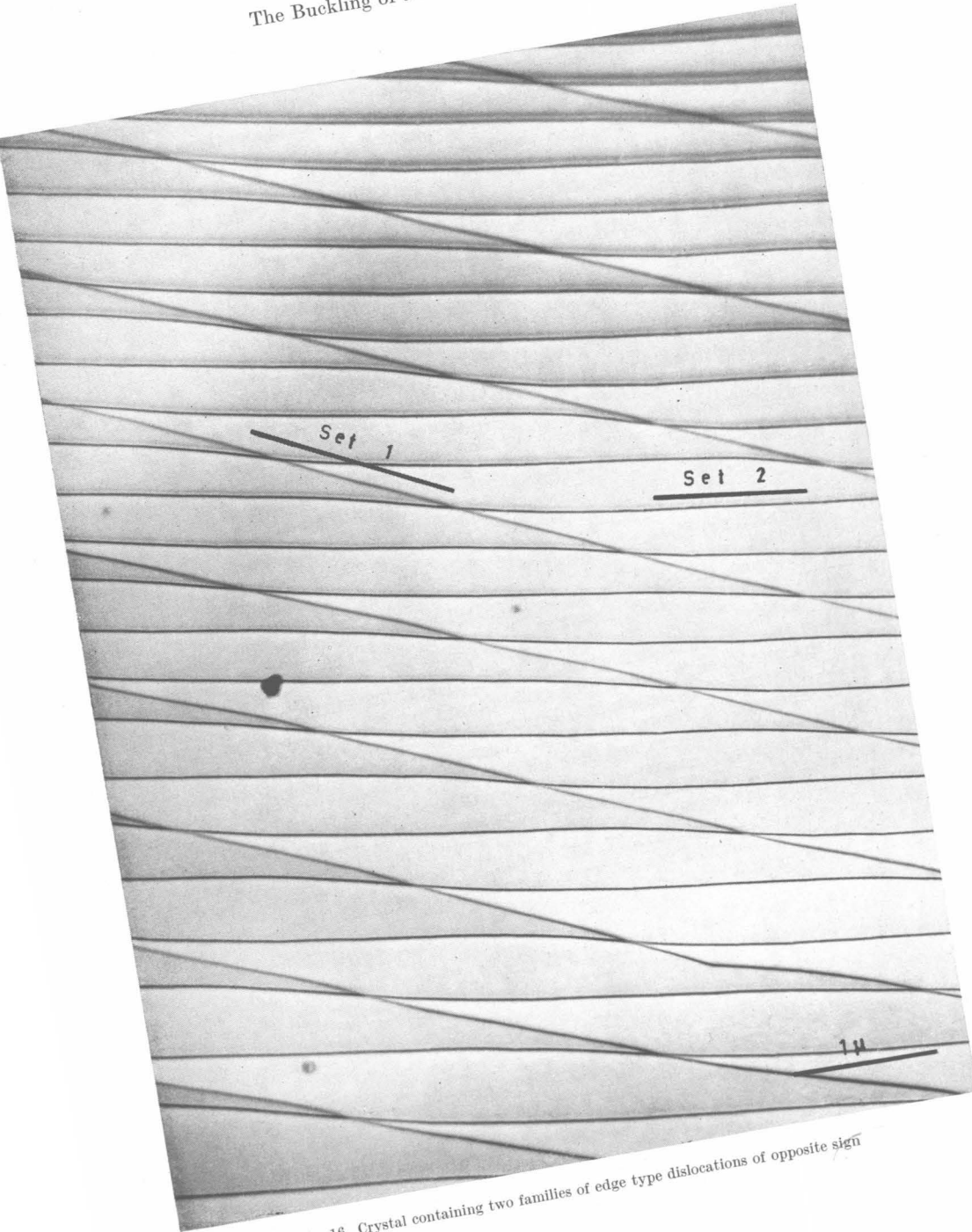
The Buckling of a Thin Plate

Fig. 16. Crystal containing two families of edge type dislocations of opposite sign

7. Conclusion

All the observations reported here are consistent with the given picture. It now becomes possible to determine the sign of the dislocations from the sense of buckling of the foil, i.e. by simple inspection of the sense of displacement of Kikuchi lines as the selection aperture passes over the dislocation.

The edge character can be recognized at the shade difference. Fig. 16 shows e.g. two sets of crossing dislocations with edge character. At a simple glance one can deduce that the edge component of the two sets have opposite sign. On crossing dislocations of set 1 the background becomes darker when going from bottom to top of the photograph; the reverse is true for set 2.

Acknowledgements

References

[1] J. D. Eshelby, Phys. Rev. 91, 755 (1953); J. appl. Phys. 24, 176 (1953); Phil. Mag. 3, 440 (1958).
[2] W. W. Webb, R. D. Dragsdorf and W. D. Forgeng, Phys. Rev. 108, 498 (1957).
[3] W. W. Webb and W. D. Forgeng, J. appl. Phys. 28, 1449 (1957); Acta metall. 6, 462 (1958).
[4] P. Delavignette and S. Amelinckx, Phil. Mag. 5, 729 (1960).
[5] S. Amelinckx and W. Dekeyser, Solid State Phys. 8, Academic Press 1959 (p. 331).
[6] H. D. Dietze and G. Leibfried, Diplomarbeit, Göttingen 1949.
[7] H. Hashimoto, A. Howie and M. J. Whelan, Proc. Eur. Reg. Conf. on El. Mic., Delft 1960; (Ed. Howink and Spit 1961) (p. 207).
[8] R. Gevers, private communication, to be published.
[9] W. Kossel and G. Möllenstedt, Naturwissenschaften 26, 660 (1938); Ann. Phys. (Leipzig) 36, 113 (1939).
[10] M. J. Whelan, J. Inst. Met. 87, 392 (1959).
[11] S. Amelinckx and P. Delavignette, J. appl. Phys. 31, 2126 (1960).
[12] A. Kelly, private communication.